Water Research 299 (2026) 125875

Contents lists available at ScienceDirect

Water Research

journal homepage: www.elsevier.com/locate/watres

Discovery of halogenated cyclopentene-diones as a new class of toxic disinfection byproducts from reaction of phenols with secondary disinfectants

Mengge Fan [a], Jialing Luo [b], Yanpeng Gao [b], Huang Huang [a], Junlang Qiu [a,*], Xin Yang [a,*]

[a] School of Environmental Science and Engineering, Guangdong Provincial Key Laboratory of Environmental Pollution Control and Remediation Technology, Sun Yat-sen University, Guangzhou 510275, China

[b] Guangdong Key Laboratory of Environmental Catalysis and Health Risk Control, Guangzhou Key Laboratory Environmental Catalysis and Pollution Control, School of Environmental Science and Engineering, Institute of Environmental Health and Pollution Control, Guangdong University of Technology, Guangzhou 510006, China

HIGHLIGHTS

- Discovered toxic halo-CDs from secondary disinfection of phenols with HOBr/HOI.
- Prioritized and identified halo-CDs via cytotoxicity-based EDA method.
- Proposed formation pathways of halo-CDs under secondary disinfections.
- Confirmed halo-CDs presence in disinfected real waters and their health risks.

GRAPHICAL ABSTRACT

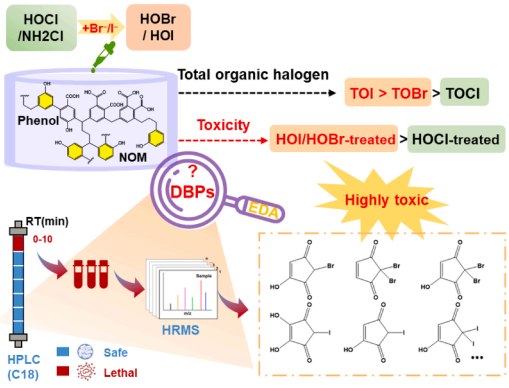

ARTICLE INFO

Keywords:
Secondary disinfectants
Disinfection byproducts
Halo-cyclopentene-diones
Effect-directed analysis
High-resolution mass spectrometry
Toxicity

ABSTRACT

The oxidation of Br^- and I^- during chlorination leads to the generation of secondary disinfectants, hypobromous acid (HOBr) and hypoiodous acid (HOI), which subsequently results in the formation of highly toxic halogenated disinfection byproducts (DBPs). This study reported the formation of previously overlooked halogenated cyclopentene-diones (halo-CDs) from phenols upon reaction with HOBr and HOI. The known DBPs were found to account for only a minor portion of total organic halogen in reaction of phenols with secondary disinfectants, warranting further investigation of elucidating the unknown fraction. To prioritize and identify the unknown toxic DBPs, the effect-directed analysis (EDA) was applied to the reaction mixtures of model phenols with secondary disinfectants. By integrating cytotoxicity-directed fractionation and high-resolution mass spectrometry, a series of halo-CDs were prioritized and identified. These compounds were then confirmed in simulated and real source waters treated by secondary disinfectants, suggesting their common occurrence in disinfected drinking water. Based on the experimental observation of intermediates, the formation pathways of halo-CDs were theoretically proposed to involve sequential halogenation, hydrolysis, hydroxylation, oxidative ring-cleavage,

* Corresponding authors.
E-mail addresses: qiujlang@mail.sysu.edu.cn (J. Qiu), yangx36@mail.sysu.edu.cn (X. Yang).

https://doi.org/10.1016/j.watres.2026.125875
Received 2 February 2026; Received in revised form 20 March 2026; Accepted 3 April 2026
Available online 4 April 2026
0043-1354/© 2026 Elsevier Ltd. All rights are reserved, including those for text and data mining, AI training, and similar technologies.

decarboxylation, and cyclization. Computational toxicity assessments demonstrated that the identified halo-CDs would pose considerable health risks. The findings herein implied that a large number of toxic DBPs might remain covered due to the inadequate focus on secondary disinfectants, which underscored the urgent need to broaden identification of DBPs beyond reaction involving primary disinfectants.

1. Introduction

Drinking water disinfection is essential for public health protection, yet it inevitably results in the formation of disinfection by-products (DBPs) through reactions between disinfectants (e.g., hypochlorous acid (HOCl)) and constituents present in source waters (Dejaeger et al., 2022; Dong et al., 2019). During disinfection, Br^- and I^- can be oxidized by primary disinfectants to form hypobromous acid (HOBr) and hypoiodous acid (HOI), which act as secondary disinfectants and further participate in DBP formation (Heeb et al., 2014; Li et al., 2020). In source waters, Br^- and I^- concentrations typically range from 5 to 500 μg L^{-1} and 0.5 to 100 μg L^{-1}, respectively. Natural processes such as seawater intrusion can elevate Br^- levels from 42.5 μg L^{-1} to 1100 μg L^{-1} in coastal groundwater (Chowdhury, 2022). Anthropogenic activities, including oil and gas brine disposal, can increase I^- concentrations up to 28,000 μg L^{-1} in impacted surface waters (Harkness et al., 2015). Elevated Br^- and I^- levels promote the formation of secondary disinfectants (e.g., HOBr and HOI) and subsequently influence DBP speciation and yields (Dorji et al., 2020; Harkness et al., 2015; Sharma et al., 2019). The role of these secondary disinfectants is often significant yet comparatively less characterized than that of primary disinfectants.

Compared to the primary disinfectant HOCl, HOBr, and HOI generally exhibit higher reactivity toward organic compounds, leading to altered and often enhanced DBP formation (Criquet et al., 2015; Dong et al., 2019). Reactions with HOBr and HOI significantly promote the formation of brominated DBPs (Br-DBPs) and iodinated DBPs (I-DBPs), including trihalomethanes (THMs) and haloacetic acids (HAAs), which typically possess higher cytotoxicity and genotoxicity than their chlorinated analogs (Liu et al., 2017; Wang et al., 2014; Yang et al., 2014). Beyond these known Br- and I-DBPs, a substantial fraction of the total organic halogen (TOX) formed during bromination and iodination comprises unidentified compounds, representing a significant pool of unknown DBPs (Hua et al., 2006; Zhu and Zhang, 2016). For example, HOBr reactions can yield numerous unidentified Br-DBPs, such as brominated aliphatic carboxylic acids and aromatic phenolic acids (Lu et al., 2025), while HOI reactions produce iodinated phenols and quinone-like structures under various pH conditions (Pan et al., 2021). Nevertheless, the comprehensive product profiles and reaction mechanisms between organic compounds and secondary disinfectants remain insufficiently elucidated. Previous studies suggested that HOBr possessed greater electrophilic substitution propensity but lower oxidative capacity than HOCl toward aromatic compounds (Westerhoff et al., 2004); in contrast, HOI preferentially reacted with highly aromatic structures to form a larger fraction of unknown I-DBPs, while less aromatic precursors favor regulated iodinated THMs and HAAs (Postigo and Zonja, 2019). These distinct reactivity patterns imply that DBP formation pathways involving secondary disinfectants likely differ from chlorination and warrant systematic investigation.

As the dominant organic component in source water (1–10 mg C L^{-1}), natural organic matter (NOM) serves as the key DBP precursor and contributes crucially to the formation of various DBPs (Connolly et al., 2020; Dejaeger et al., 2022). Within NOM, phenolic moieties are considered particularly reactive DBP precursors owing to their electron-rich aromatic structures (Ayatollahi et al., 2012; Chuang et al., 2015; Gallard and Von Gunten, 2002). Quantitative analyses indicate that phenolic groups constitute 13 %–30 % of the carbon in humic substances, underscoring their importance in DBP formation during water treatment (Ritchie and Perdue, 2003). Extensive research has established phenols as critical precursors for regulated DBPs, with their substitution patterns strongly influencing DBP yields and speciation (Bond et al., 2012; Boyce and Hornig, 1983; Chaidou et al., 1999; Gallard and Von Gunten, 2002; Heasley et al., 1993). For instance, THMs formation during chlorination is highly structure-dependent (Bond et al., 2012; Boyce and Hornig, 1983). Resorcinol (Res) can yield > 85 % trichloromethane (TCM), whereas catechol and hydroquinone produce only trace levels (< 0.5 %) of TCM under similar conditions (e.g., disinfectant-to-precursor molar ratio of 6–8, pH 4, 7, and 10, and a reaction time of 24 h) (Boyce and Hornig, 1983).

The reaction of HOBr and HOI with aromatic precursors generates a complex and largely unidentified mixture of DBPs. Direct analysis characterization is challenged by the diversity, structural complexity, and instability of these unknown compounds, complicating their detection by conventional methods (Kimura et al., 2019). Consequently, a significant portion of the toxicological burden associated with disinfection remains chemically uncharacterized, impeding accurate risk assessment. To address this gap, effect-directed analysis (EDA) provides a strategic, bioassay-guided framework. By coupling high-resolution fractionation with in vitro toxicity assays, EDA enables the prioritization and identification of bioactive components without requiring exhaustive non-target screening (Brack, 2003; Dong et al., 2020). Recent EDA applications have successfully identified potent DBPs missed by routine monitoring, such as iodinated nitrobenzonitrile and imidazole derivatives (Ouyang et al., 2024; Yang et al., 2025), demonstrating the utility of this approach for elucidating toxic unknown DBPs from secondary disinfectant reactions.

This study therefore aimed to systematically evaluate the formation of known and unknown DBPs from reactions between secondary disinfectants (HOBr and HOI) and phenols. An integrated EDA approach was employed to identify unknown toxic DBPs. The strategy combined bioassay-directed fractionation with high-resolution mass spectrometry (HRMS) to isolate bioactive fractions and elucidate the structures of key toxicants. The environmental relevance of the identified DBPs was assessed by screening for their occurrence in simulated and real source waters. Finally, the potential health risks associated with these compounds were evaluated using quantitative structure–activity relationship (QSAR) models and the Danish (Q)SAR database.

2. Materials and methods

2.1. Chemicals and reagents

The phenols selected are listed in Table S1, along with their structural characteristics. The stock solution of free chlorine (1000 mg L^{-1}) was prepared by diluting 5 % sodium hypochlorite (NaOCl; Sigma-Aldrich, the USA) with ultrapure water (18.2 mΩ cm). All chemicals and reagents are of analytical grade or higher. Detailed information on chemical sources and purities is provided in Text S1. HOBr and HOI stock solutions were prepared and quantified as described in Text S2. Chinese hamster ovary (CHO-K1) cells, obtained from Procell Life & Technology Co., Ltd., were maintained in Dulbecco's Modified Eagle Medium (DMEM; PM150210) supplemented with 10 % fetal bovine serum (FBS; 164,210-500) and 1 % penicillin-streptomycin (P/S; PB180120), and incubated at 37 °C under 5 % CO_2.

2.2. Disinfection experiments

All disinfection tests were performed in 1 L amber glass bottles filled to exclude headspace and kept in the dark at 25 ± 1 °C. The solution pH

was maintained at 8.0 using 5.0 mM phosphate buffer, as this pH optimizes the reactivity of both HOX species (Bichsel and Von Gunten, 2000; Gallard et al., 2003; Hung et al., 2017) and phenoxide ions (Tee et al., 1989) while remaining within the environmentally relevant range for source waters (Qiao et al., 2016). Disinfection was initiated by adding each disinfectant (HOCl, HOBr, and HOI) at a molar ratio of 10:1 relative to the phenols (e.g., 100 μM HOCl *v.s.* 10 μM phenol). After 24 h of reaction, residual disinfectant was quantified and immediately quenched using a 1.5-fold molar excess of ascorbic acid prior to DBP analysis.

To simulate environmentally relevant disinfection scenarios, a solution containing 5 mgC L^{-1} NOM buffered in 5 mM phosphate buffer (pH 8.0) was treated with HOCl in the presence or absence of 0.5 mg L^{-1} Br^-. In addition, filtered real surface water collected from the Pearl River was chlorinated to model real-world drinking water treatment. The resulting samples were concentrated and analyzed by HRMS to identify and characterize unknown halogenated DBPs.

2.3. Analytical methods

2.3.1. Determination of known DBPs and TOX

Three THMs (TCM, tribromomethane (TBM), and triiodomethane (TIM)) and nine HAAs (monochloroacetic acid (MCAA), dichloroacetic acid (DCAA), trichloroacetic acid (TCAA), monobromoacetic acid (MBAA), dibromoacetic acid (DBAA), tribromoacetic acid (TBAA), monoiodomoacetic acid (MIAA), diiodoacetic acid (DIAA), and triiodoacetic acid (TIAA)) were analyzed according to modified USEPA Methods 551.1/552.3 (Table S2), as detailed in our previous work (Zhong et al., 2019). Sample extraction and analytical procedures are provided in Text S3. TOX, including its chlorine-, bromine-, and iodine-specific fractions (TOCl, TOBr, and TOI), was measured following the methods described in Text S4. Each experimental condition was performed in triplicate ($n = 3$) to ensure reproducibility.

2.3.2. Toxicity assessment and fractionation of water samples

Each water sample was concentrated by solid phase extraction using CNW HLB cartridges (China), the procedure is fully described in Text S5. Cytotoxicity was evaluated in CHO-K1 cell with cells using the ACEA Biosciences xCELLigence Real-Time Cell Analysis system (the USA), following our previously established protocols (Fan et al., 2022). Briefly, 50 μL of sample concentrate (reconstituted in cell culture medium) was added in triplicate to 150 μL of cell suspension in three parallel groups. Additional experimental details are provided in Text S6.

To identify specific toxic constituents, concentrated extracts were fractionated prior to toxicological and chemical analysis. Fractionation was performed using a Shimadzu LC20 high-performance liquid chromatograph (HPLC; Japan) system equipped with a Shimadzu Shim-pack PREP-ODS preparative reversed-phase C18 column (20 mm × 25 cm × 5 μm; Japan). The mobile phase consisted of (A) water and (B) methanol, each containing 0.25 % formic acid, under gradient conditions specified in Text S7. Seven fractions were collected at 10 min intervals (20 mL each), concentrated under a gentle nitrogen stream, and lyophilized. The resulting residues were reconstituted for subsequent toxicity tests and HRMS analysis.

To characterize the hydrophobicity distribution of compounds in the collected fractions, a set of 13 halogenated DBPs (including 6 aliphatic and 7 aromatic compounds with varied log *K*ow values) were fractionated using the same preparative HPLC method. Based on their retention times (RTs), a threshold of 40 min was established to distinguish between aliphatic and aromatic halo-DBPs (Fig. S1). Accordingly, fractions F1–F4 (RT: 0–40 min) predominantly contained aliphatic DBPs, while fractions F5–F7 (RT: 40–70 min) were mainly enriched in aromatic species.

2.3.3. Identification of unknown DBPs

Fractions showing pronounced cytotoxic effects (> 50 % inhibition of CHO cell growth) were subjected to structural analysis using an Agilent 1290 Infinity II liquid chromatograph coupled to an Agilent 6545 quadrupole time-of-flight mass spectrometer (LC-Q-TOF MS; Singapore). Separation was performed on an Agilent ZORBAX RRHD Eclipse Plus C18 column (2.1 mm × 150 mm × 1.8 μm; the USA) maintained at 30 °C. The mobile phases consisted of (A) water and (B) methanol, both containing 0.1 % formic acid, delivered at a flow rate of 0.15 mL min^{-1}. The injection volume was 10 μL. MS detection was conducted in negative ionization mode using a dual jet stream electrospray ionization (ESI) source, with data acquired in 2 GHz extended dynamic range over a mass range of 50–1700. Detailed LC gradient and MS operating parameters are provided in Text S8.

2.4. Prediction of potential health risks

Developmental toxicity (Eq. 2–1) and growth inhibition potential (Eq. 2–2) of the identified DBPs were predicted using previously established QSAR models (Liu and Zhang, 2014; Yang and Zhang, 2013):

$$\log EC_{50}^{-1} = 0.3535\log P + 0.7243pKa - 1.7101E_{LUMO} - 1.4132E_{HUMO} - 22.5945 \quad (2\text{–}1)$$

$$\log EC_{50}^{-1} = 0.7931\log P + 0.7277pKa + 0.0050MTI - 13.2026 \quad (2\text{–}2)$$

The models incorporated the following molecular descriptors: logP (octanol-water partition coefficient), p*K*a (dissociation constant), E_{LUMO} (energy of the lowest unoccupied molecular orbital), E_{HOMO} (energy of the highest occupied molecular orbital), and MTI (molar topological index). These descriptors were computed as follows: log P was obtained using KOWWIN (v1.68), p*K*a with MolGpKa, E_{LUMO} and E_{HOMO} via Multiwfn, and MTI using Chem3D Ultra. A detailed rationale for descriptor selection and their correlation with developmental toxicity is provided in Text S9.

Potential human health risks, including skin sensitization, respiratory sensitization, carcinogenicity, and mutagenicity, were evaluated using the Danish (Q)SAR database (Danish(Q)Sar, 2015; Rosenberg et al., 2016). The model outputs a probability value (*p*) between 0 and 1 for each endpoint, where values closer to 1 indicate a higher likelihood of adverse effects.

3. Results and discussion

3.1. Formation of known DBPs

The formation yields of known DBPs, THMs and HAAs, were quantified from reactions between three disinfectants (HOCl, HOBr, and HOI) and a series of phenols. Phenols were categorized into three groups based on their hydroxyl substitution patterns, including the number of hydroxyl groups and their relative positions: monohydroxy phenols (Group I), *ortho-*/*para*-substituted polyhydroxy phenols (Group II), and *meta*-substituted polyhydroxy phenols (Group III). As shown in Fig. 1(a), THM yields varied substantially among these groups. Group I phenols generated moderate THM yields (0.2 %–37 %). Group II phenols produced comparatively lower yields (0.3 %–15 %), consistent with their reported tendency to undergo oxidation to quinones rather than halogenation (Criquet et al., 2015). In contrast, Group III phenols exhibited the highest THM yields (13 %–94 %), reflecting the strong activation of aromatic ring by *meta*-hydroxyl groups toward electrophilic substitution (Bond et al., 2012; Gallard and Von Gunten, 2002).

Distinct disinfectant-specific THM formation trends were evident within each phenolic group. For Group I phenols, HOBr produced higher TBM yields than HOCl or HOI, attributable to its stronger halogenation propensity relative to HOCl and greater oxidative power compared to HOI (Liu et al., 2022). Conversely, for Group III phenols, the lowest THM yields were observed with HOI, likely because the *meta*-substituted

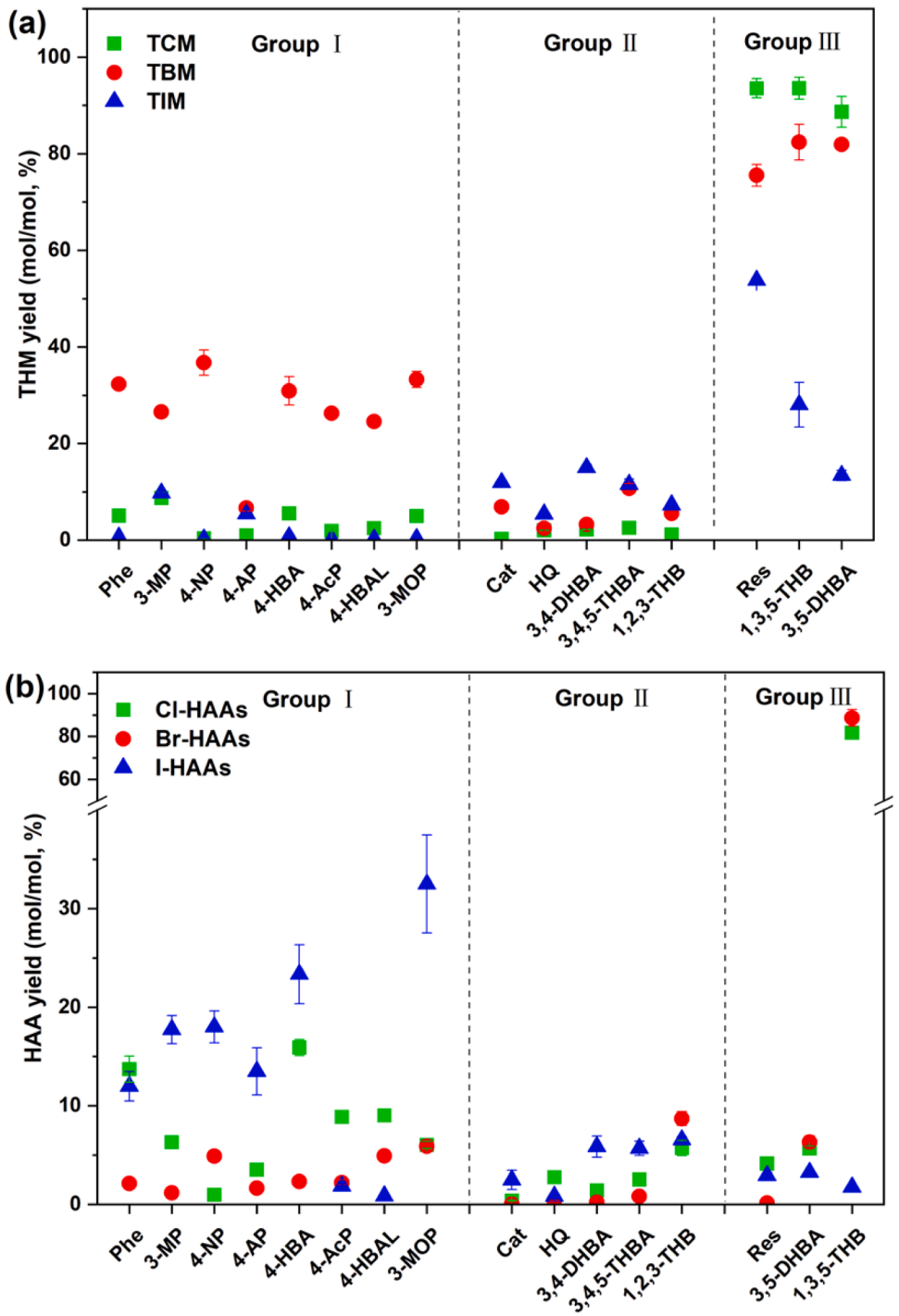

Fig. 1. (a) THM and (b) HAA yields (mol DBP/mol phenol, %) in reactions of phenols treated by HOX (X = Cl/Br/I). Experiment conditions: $[HOCl]_0 = [HOBr]_0 = [HOI]_0 = 100$ μM, $[phenols]_0 = 10$ μM, pH = 8, reaction time = 24 h. Noted that error bars represent the standard deviation based on triplicate analyses.

structure facilitated initial halogenation, but the subsequent oxidative ring-cleavage was hindered by the relatively weak oxidizing capacity (Liu et al., 2022).

Given the parallel formation trends observed for trihaloacetic acids (THAAs) and dihaloacetic acids (DHAAs), their combined yields (total HAAs) are presented in Fig. 1(b) (individual species yields are provided in Fig. S2). Monohaloacetic acids (MHAAs) were also monitored but remained below the detection limit, as the molar excess of disinfectant favors the formation of DHAAs and THAAs. Group I phenols yielded 0.7 %–30.7 % HAAs, whereas most Group II and Group III phenols produced low HAA yields (< 10 %). A notable exception was 1,3,5-trihydroxybenzene (1,3,5-THB), which exhibited approximately 20-fold higher chlorinated HAA formation potential than resorcinol (81.8 % ± 2.3 % *v.s.* 4.2 % ± 0.2 %). This marked difference can be attributed to the lower p*K*a of 1,3,5-THB, which increases the fraction of highly reactive deprotonated species, and its higher $SUVA_{254}$ value, reflecting greater aromaticity that promotes ring cleavage upon electrophilic attack (Chang et al., 2006). For 1,3,5-THB, brominated HAA yields were similarly elevated, while iodinated HAA yields remained low, in line with the weaker oxidizing power of HOI (Liu et al., 2022). The generally low HAA yields from Group II phenols aligned with their predominant oxidation pathway to quinones (Criquet et al., 2015), while the high

THM-forming propensity of Group III phenols likely limited their conversion to HAAs.

TOX yields (mol halogen mol^{-1} phenol) were also determined. Unknown TOX (UTOX), calculated by subtracting the halogen incorporated into THMs and HAAs, accounted for > 65 % of the TOX formed (Fig. 2), consistent with previous studies (Fang et al., 2023). Notably, for a given phenol, both TOX and UTOX yields followed the order HOI > HOBr > HOCl. This trend correlated with the greater electrophilic substitution propensity of HOI, as indicated by its more negative Hammett slope ($\rho_{HOI} = -7.1$) compared to HOBr ($\rho_{HOBr} = -3.3$) and HOCl ($\rho_{HOCl} = -3.0$) (Lee et al., 2005).

3.2. Cytotoxicity-based prioritization of fractions

The distinct DBP profiles formed from different phenol-disinfectant combinations necessitated a targeted approach to identify key toxicants. Given that aromatic DBPs constitute 49 %–67 % of TOX in chlorinated waters (Han et al., 2021), understanding the transformation of aromatic intermediates to aliphatic DBPs is crucial. To balance analytical depth with feasibility, three representative phenols from each phenol group, including phenol (Phe, Group I), hydroquinone (HQ, Group II), and Res (Group III), were selected for EDA after treatment with HOCl, HOBr, or HOI.

First, the cytotoxicity of all nine reaction mixtures (three phenols treated with three disinfectants, respectively) was assessed to prioritize samples for fractionation. As shown in Fig. 3(a), HOCl-treated samples consistently exhibited lower cytotoxicity than HOBr- or HOI-treated samples, attributable to both lower overall TOX formation and the generally lower toxicity of chlorinated versus brominated/iodinated analogues (Wagner and Plewa, 2017). At a 50-fold concentration factor, HOCl-treated Phe showed no detectable cytotoxicity. In contrast, HOBr- and HOI-treated Phe caused remarkable growth inhibition of 94.0 % ± 0.0 % and 90.0 % ± 5.8 %, respectively. For HQ and Res, pronounced cytotoxic responses (growth inhibition of 89.7 % ± 5.8 % and 94.8 % ± 0.8 %) were observed only with HOI treatment, whereas inhibition rates for HOCl- and HOBr-treated samples remained below 20 %. Consequently, four treatment groups exhibiting significant toxicity, including HOBr-treated Phe, HOI-treated Phe, HOI-treated HQ, and HOI-treated Res, were selected for further fractionation.

Following fractionation procedure was conducted to aforementioned four treating groups, and the fractions with highest cytotoxic effect of each treating group were selected out for the subsequent HRMS analysis. The cytotoxicity distribution across fractions revealed distinct patterns: for HOBr-treated Phe, toxicity was concentrated in F1 (Fig. 3(b)). For HOI-treated Phe, the highest toxicity resided in fractions F5 and F6 (Fig. 3(c)). For both HOI-treated HQ and HOI-treated Res, toxicity was again highest in F1 (Fig. 3(d, e)). These five highly toxic fractions (F1 from HOBr-treated Phe, HOI-treated HQ, and HOI-treated Res, and F5–F6 from HOI-treated Phe) were subsequently analyzed by LC-Q-TOF MS for DBP identification.

3.3. HRMS identification of unknown DBPs

To inform the polarity characteristics of unknown DBPs, model aliphatic and aromatic DBPs were fractionated using the same protocol. Results indicated that fractions F1–F4 primarily contained aliphatic DBPs, while fractions F5–F7 were enriched with aromatic DBPs (Fig. S1). Therefore, the identification of unknown DBPs in the fractions could be directed in the perspective of aromatic or aliphatic components.

3.3.1. HOI-treated Phe

F5 and F6 from HOI-treated Phe were subjected to characterization with focus on aromatic compounds. The LC chromatogram of the HOI-

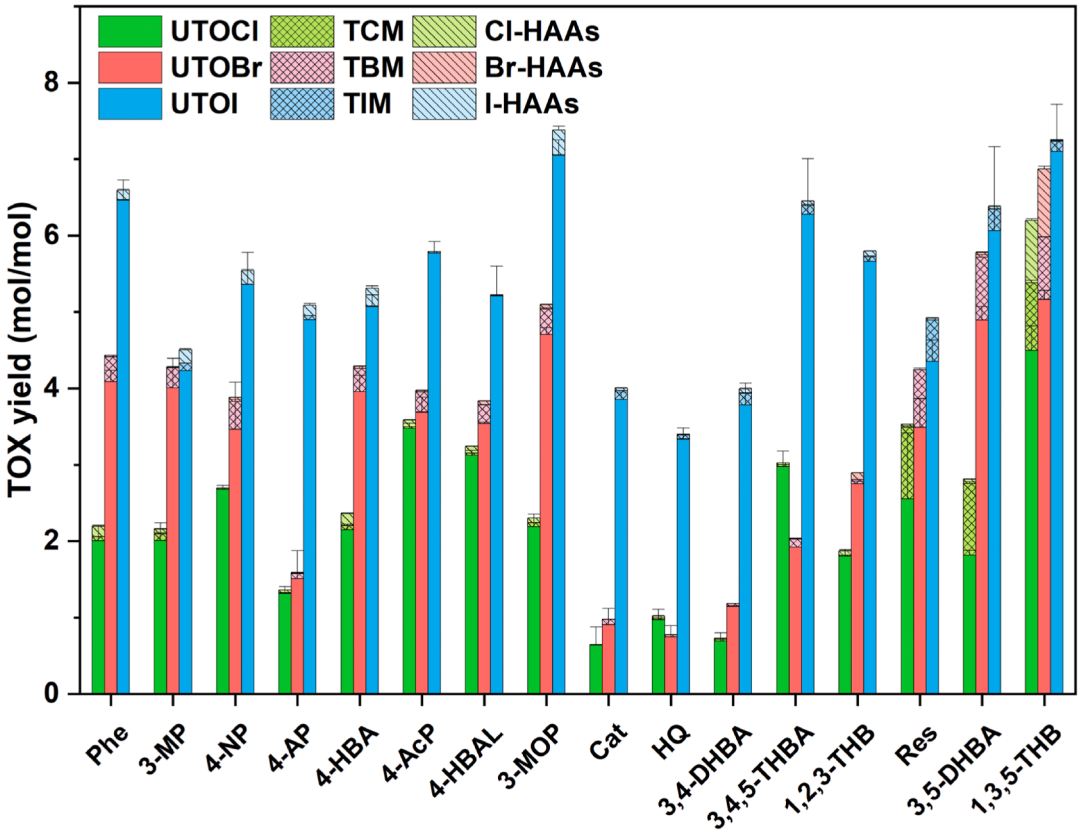

Fig. 2. Unknown TOX yields (mol halogen/mol phenol) in reactions of phenols treated by HOX (X = Cl/Br/I). Experiment conditions: $[HOCl]_0 = [HOBr]_0 = [HOI]_0 = 100$ μM, $[phenols]_0 = 10$ μM, pH = 8, T = 25 ± 1 °C, reaction time = 24 h. Noted that error bars represent the standard deviation based on triplicate analyses.

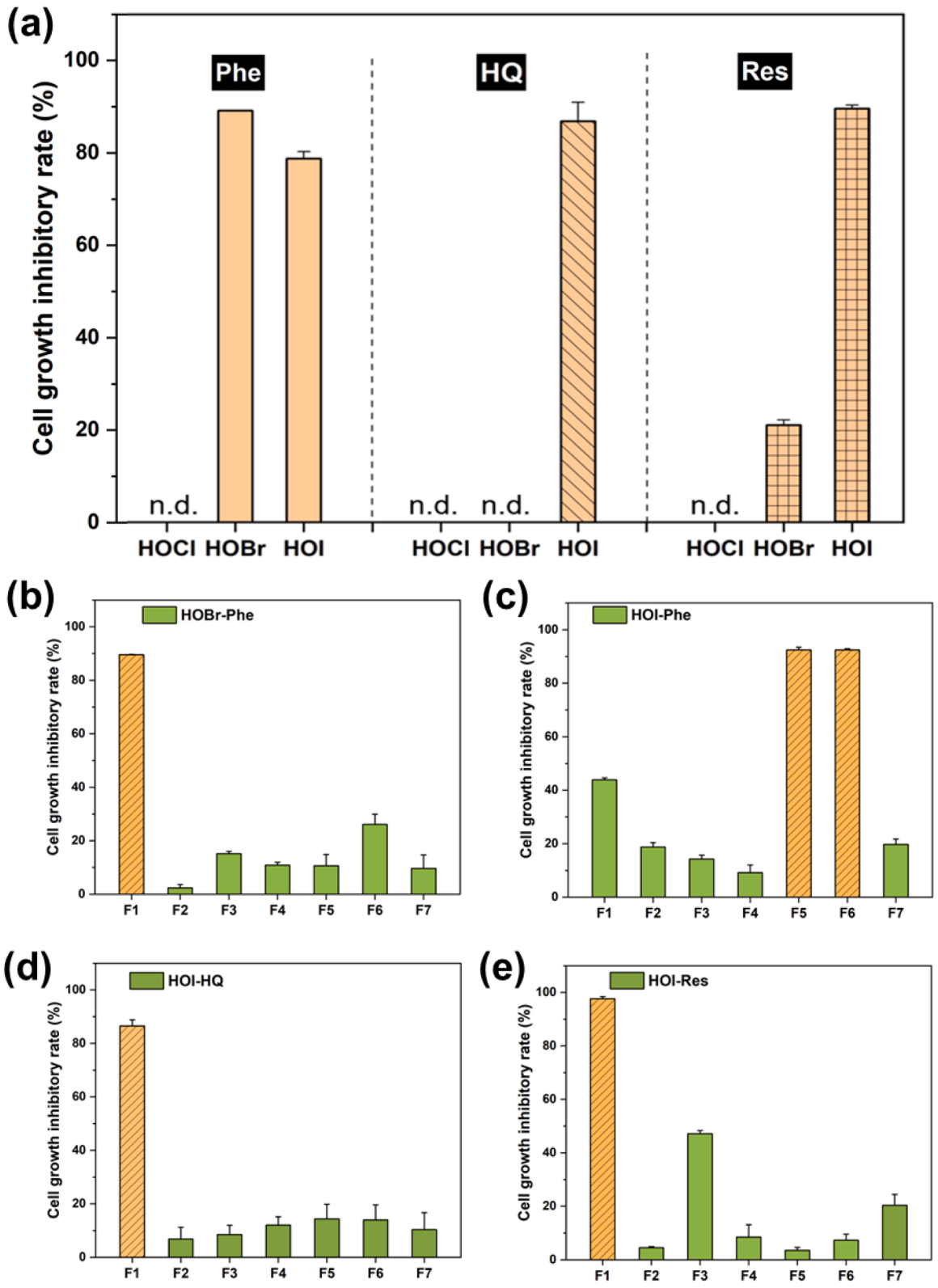

Fig. 3. (a) Overall cytotoxicity of Phe, HQ, and Res treated with HOCl/HOBr/HOI; (b–e) fractional cytotoxicity of HOBr-treated Phe, HOI-treated Phe, HOI-treated HQ, and HOI-treated Res. Experiment conditions: $[HOCl]_0 = [HOBr]_0 = [HOI]_0 = 100$ μM, $[phenols]_0 = 10$ μM, pH = 8, T = 25 ± 1 °C, reaction time = 24 h. CHO cell exposure time = 48 h, concentration factors are 50 for overall cytotoxicity and 300 for fractional cytotoxicity. Noted that error bars represent the standard deviation based on triplicate analyses, n.d. means no observable cytotoxic effects were detected.

treated Phe sample exhibited multiple overlapping peaks in the 40–60 min window (Fig. S3(a)), corresponding to fractions F5 and F6. Given the high similarity of their total ion chromatograms (Fig. S3(b)), F6 was selected for detailed discussion. The dominant species was identified as 2,4,6-triiodophenol (2,4,6-TIP; RT 17.2 min, observed *m/z* 470.7247; theoretical *m/z* 470.7240; Δ = 1.7 ppm) based on its accurate mass ($[C_6H_2I_3O]^-$, *m/z* 470.7247) and characteristic MS/MS fragment corresponding to an iodine radical loss (*m/z* 126.9048) (Fig. 4(a)). Its high extraction ion chromatogram abundance (~7×10^6) significantly exceeded that of co-eluting diiodophenol (~1×10^6) and monoiodophenol (~1.1×10^4) (Fig. S4(a, b)), confirming 2,4,6-TIP as the major aromatic toxicant, consistent with previous reports (Liu et al., 2022).

3.3.2. HOBr-treated Phe, HOI-treated HQ, and HOI-treated Res

F1 from HOBr-treated Phe, HOI-treated HQ, and HOI-treated Res were subjected to characterization with focus on aliphatic compounds. HRMS analysis of the F1 fractions focused on compounds with ≤5 carbon atoms, consistent with ring-cleavage products. Several 5-carbon brominated and iodinated compounds with a double-bond equivalent (DBE) of 4 were identified and proposed as halogenated cyclopentenediones (halo-CDs) based on accurate mass, isotopic patterns, fragmentation, and hydrophilicity (log *K*ow).

In F1 fraction of HOBr-treated Phe, five brominated compounds were identified (Table 1). For example, B1 ($C_5HBr_3O_3$; RT 24.6 min, observed *m/z* 344.7425; theoretical *m/z* 344.7403; Δ = 6.4 ppm) exhibited an isotopic cluster at *m/z* 345/347/349/351 with an isotopic abundance ratio of 1:3:3:1, indicative of three bromine atoms (Fig. 4(b)). In its MS/MS spectrum, neutral losses of 28 Da (CO) and 44 Da (CO_2) supported its assignment as 2,2,4-tribromo-5-hydroxy-4-cyclopentene-1,3-dione. The structural assignment was supported by log *K*ow prediction: the calculated value for this structure (0.5) falls within the log *K*ow range of fraction F1 (0.34–1.44), consistent with its elution profile in EDA fractionation. Similar analyses identified B2–B5 as related brominated derivatives (Fig. S5, Table S3).

In F1 fraction of HOI-treated HQ, B6 ($C_5H_3IO_4$; RT 40.7 min, observed *m/z* 313.9306; theoretical *m/z* 313.9293; Δ = 4.2 ppm) was identified as a monoiodinated di-hydroxy cyclopentene-dione based on its formate adduct mass and characteristic fragment ions (Fig. 4(c)). Specifically, the accurate mass corresponded to the molecular formula $[C_5H_3IO_4+HCOO]^-$, which referred to the formate adduct of $C_5H_3IO_4$. Its MS/MS spectrum showed a neutral losse of 127.9 Da (HI), indicating the substitution of iodine atoms, which is a diagnostic fragmentation for iodinated byproducts. Then B6 was proposed as 4-iodo-2,5-dihydroxy-4-cyclopentene-1,3-dione.

In F1 fraction of HOI-treated Res, B7 and B8 were identified as mono- and di-iodinated hydroxy cyclopentene-diones, respectively. Taken B7 ($C_5H_3IO_3$; RT 41.9 min, observed *m/z* 238.9206; theoretical *m/z* 238.9187; Δ = 6.6 ppm) as an example, its accurate mass corresponded to the molecular formula $C_5H_2IO_3^-$. Its MS/MS spectrum showed neutral losses of 28 Da (CO) and 144 Da (CH_3I), indicative of carbonyl and iodoalkane-like functionalities in cyclopentene-dione structure (Fig. 4 (d)). Therefore, B7 was proposed as 4-iodo-5-hydroxy-4-cyclopentene-1,3-dione based on the accurate mass in MS^1 and fragments in MS/MS. Similarly, B8 ($C_5H_2I_2O_3$; RT 42.2 min, observed *m/z* 336.8213; theoretical *m/z* 336.8228; Δ = 4.4 ppm) was identified to be 2,4-diiodo-5-hydroxy-4-cyclopentene-1,3-dione (Fig. S5(d)).

3.3.3. Simulated and real source waters with HOCl/HOBr

Screening of simulated and real source waters treated with HOCl/HOBr confirmed the environmental relevance of halo-CDs. Five chlorinated and chloro-bromo derivatives (B9–B13) were identified (Fig. S7, Table 2). The absence of brominated and iodinated derivatives (B1–B8) in simulated and real water samples can be attributed to the experimental conditions, which did not involve treatment with HOBr or HOI alone. Specifically, the structures of B9 ($C_5HCl_3O_3$), B10 ($C_5HBrCl_2O_3$), and B11 ($C_5HBr_2ClO_3$), identified in HOCl-treated source water, were tentatively assigned as 2,2,4-trichloro-5-hydroxy-4-cyclopentene-1,3-dione, 2,2-dichloro-5-hydroxy-4-cyclopentene-1,3-dione, and 2-chloro-5-hydroxy-4-cyclopentene-1,3-dione, respectively. Meanwhile, B10 ($C_5HBrCl_2O_3$) and B11 ($C_5HBr_2ClO_3$), detected in HOCl/HOBr-treated source water, were tentatively identified as 2,2-dichloro-4-bromo-5-hydroxy-4-cyclopentene-1,3-dione and 2-chloro-2,4-dibromo-5-hydroxy-4-cyclopentene-1,3-dione, respectively. A semi-quantitative comparison of halo-CD concentrations between real and simulated water samples would be valuable once analytical standards become available.

3.4. Toxicity assessments of halo-CDs

The potential developmental toxicity and health risks of the identified halo-CDs were evaluated using QSAR modeling. The predicted developmental toxicity, growth inhibition potentials, and physicochemical parameters were presented in Table S4. Two iodinated HCDs (B7 and B8) and one chlorinated HCD (B12) exhibited the highest predicted developmental toxicity, with EC_{50} values 3–5 orders of magnitude lower than their phenolic precursors. According to the applied model (Eq. 2–1), developmental toxicity correlated positively with p*K*a and negatively with E_{LUMO}. Specifically, p*K*a governed the ionization potential of the compound, while E_{LUMO} served as a descriptor of its relative electrophilicity. Compared to phenolic precursors, these three high-toxicity halo-HCDs (B7, B8, and B12) exhibited comparable p*K*a values but lower E_{LUMO} values, which contributed to their lower predicted EC_{50} values (i.e., higher potency). The higher predicted developmental toxicity of B7, B8, and B12 was primarily attributed to their substantially higher pKa values compared to other halo-CDs.

Expanded toxicity profiling using the Danish (Q)SAR Database revealed additional concerns (Table S5). All halo-CDs showed a high probability of skin sensitization ($p > 0.9$), exceeding the values predicted for phenols (0.68–0.77) and HAAs (0.33–0.53). Several halo-CDs (B9–B13) also exhibited elevated probabilities of severe skin irritation ($p > 0.89$) compared to phenols (0.66–0.80). Several brominated CDs (B2 and B4) and iodinated CDs (B1, B5, and B7) were also predicted to pose respiratory sensitization hazards. Moreover, enhanced carcinogenic and mutagenic potentials were also observed in some of halo-CDs. For example, chloro and chloro-bromo CDs (B9–B13) exhibited higher probabilities of liver-specific carcinogenesis (0.77–0.98) than those of phenols and Br-/I-HAAs (0.15–0.46). Besides, brominated CDs (B1 and B2) and iodinated CDs (B5–B7) showed increased mutagenicity in mouse lymphoma assays (0.79–0.95) than those of phenols (0.72–0.82) and HAAs (0.29–0.31). These integrated predictions suggested that halo-CDs generated during secondary disinfection may pose multifaceted health risks, prompting further experimental validation and regulatory consideration.

3.5. Formation mechanisms of halo-CDs

Based on the identified products, key intermediates (I, II, and IV detected in the Phe samples by HRMS; Fig. S8), and theoretical evidences (Huang et al., 2018; Pan et al., 2016), the reaction pathways for halo-CDs during HOCl/HOBr/HOI treatment were proposed. The pathways accounted for both hydroxylated (halo-HCDs) and non-hydroxylated (halo-CDs) variants (Fig. 5), including chlorinated-, bromated-, and iodinated-CDs.

The mechanism initiated with electrophilic halogenation of the phenol ring, yielding halogenated phenols (Intermediate I) (Criquet et al., 2015), which hydrolyzed to halogenated hydroquinones (Intermediate II) (Zhao et al., 2012). Oxidation produced halogenated benzoquinones (Intermediate III), followed by further hydroxylation to mono-hydroxylated benzoquinone intermediates (IV) (Huang et al., 2018). Further hydroxylation, likely through repeated halogenation-hydrolysis sequences, led to mono-hydroxylated

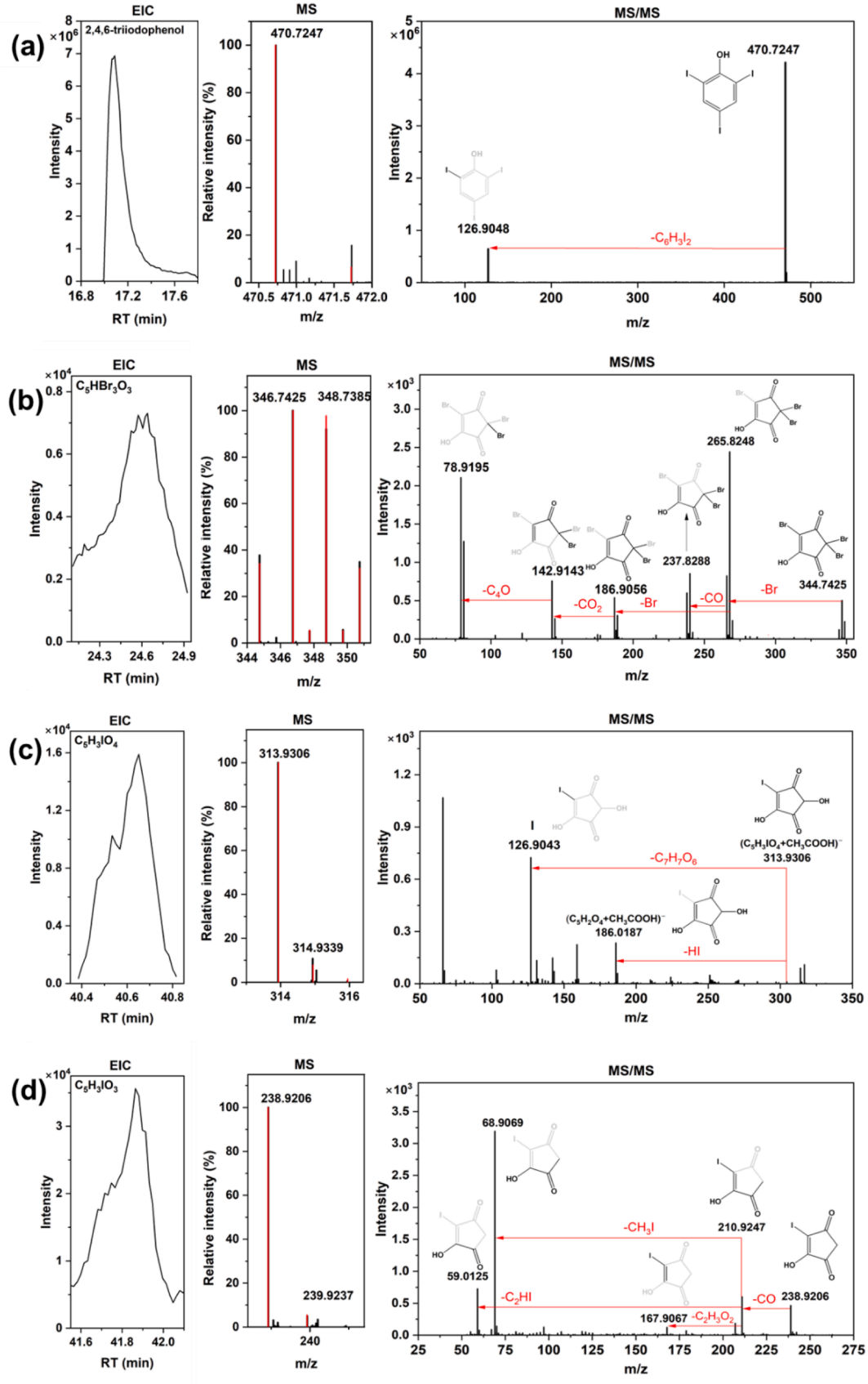

Fig. 4. EIC, MS spectra, and MS/MS spectra of template halo-CDs identified in each of the four groups: (a) 2,4,6-triiodophenol ($C_6H_3I_3O$) from HOI-treated Phe, (b) B1 ($C_5HBr_3O_3$) from HOBr-treated Phe, (c) B6 ($C_5H_3IO_4$) from HOI-treated HQ, and (d) B7 ($C_5H_3IO_3$) from HOI-treated Res. Noted that The MS spectra show the detected peaks (black) and the theoretical isotopic distributions of putatively identified compounds (red); The proposed structures and fragmentation pathways are shown in the MS/MS spectra.

Table 1
Chemical formulas and proposed structures of identified halo-CDs formed from disinfected phenols.

Group	DBP ID	Chemical formula	Proposed structure
HOBr-Phe	B1	$C_5HBr_3O_3$	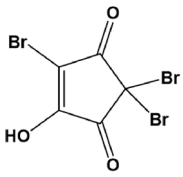
	B2	$C_5H_2Br_2O_2$	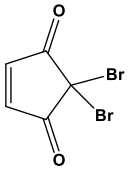
	B3	$C_5H_2Br_2O_3$	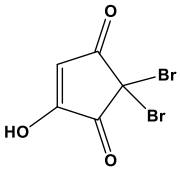
	B4	$C_5H_3BrO_3$	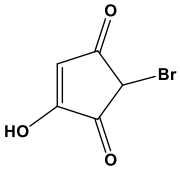
	B5	$C_5HBr_3O_2$	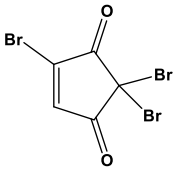
HOI-HQ	B6	$C_5H_3IO_4$	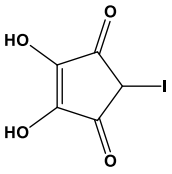
HOI-Res	B7	$C_5H_3IO_3$	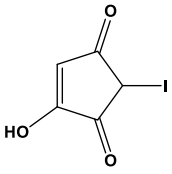
	B8	$C_5H_2I_2O_3$	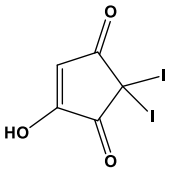

Table 2
Chemical formulas and proposed structures of identified halo-CDs formed from disinfected simulated and real source waters.

Group	DBP ID	Chemical formula	Proposed structure
HOCl- simulated source water	B9	$C_5HCl_3O_3$	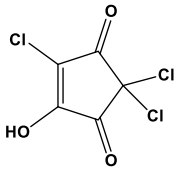
	B12	$C_5H_3ClO_3$	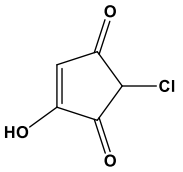
	B13	$C_5H_2Cl_2O_3$	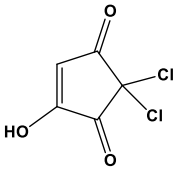
HOCl/HOBr- simulated source water	B10	$C_5HBrCl_2O_3$	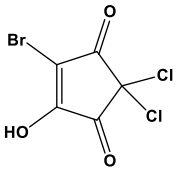
	B11	$C_5HBr_2ClO_3$	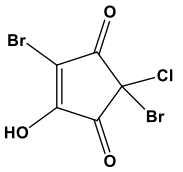
HOCl-real source water	B9	$C_5HCl_3O_3$	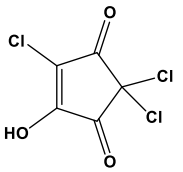

benzoquinone (intermediate IV). The subsequent branching point determined the final product class:

In halo-HCDs formation route (Fig. 5(a)), further hydroxylation of intermediate IV led to di-hydroxylated benzoquinones (intermediate Route1-IV) (Mccomas et al., 2002). Then intermediate Route1-V was formed by HOCl/HOBr/HOI addition to the di-hydroxylated benzoquinone. Following ring opening procedure transformed intermediate Route1-V to intermediate Route1-VI, which was then proceed through decarboxylation and cyclization steps to generate halo-HCDs. Detailed formation routes for representative halo-HCDs (B1, B3, and B4) were provided in Fig. S9(a–c). Intermediates in the halo-CD formation pathway (e.g., intermediate IV) may undergo ring-opening reactions to generate known DBPs such as DBAA (Huang et al., 2018). However, quantitative analysis of these potential relationships could not be performed due to the current unavailability of authentic halo-CD standards. While substitution position may influence the formation potential of halo-CDs, its impact on the underlying formation mechanism appears limited (Huang et al., 2018). Future quantitative comparisons using authentic halo-CD standards would provide further insights into these structural effects once available.

In halo-CDs formation route (Fig. 5(b)), intermediate Route2-V was directly formed by HOCl/HOBr/HOI addition to the mono-hydroxylated benzoquinone. Similar to halo-HCDs, intermediate Route2-V was oxidized by disinfectants and produced intermediate Route2-VI, which was then proceed through decarboxylation and cyclization steps to

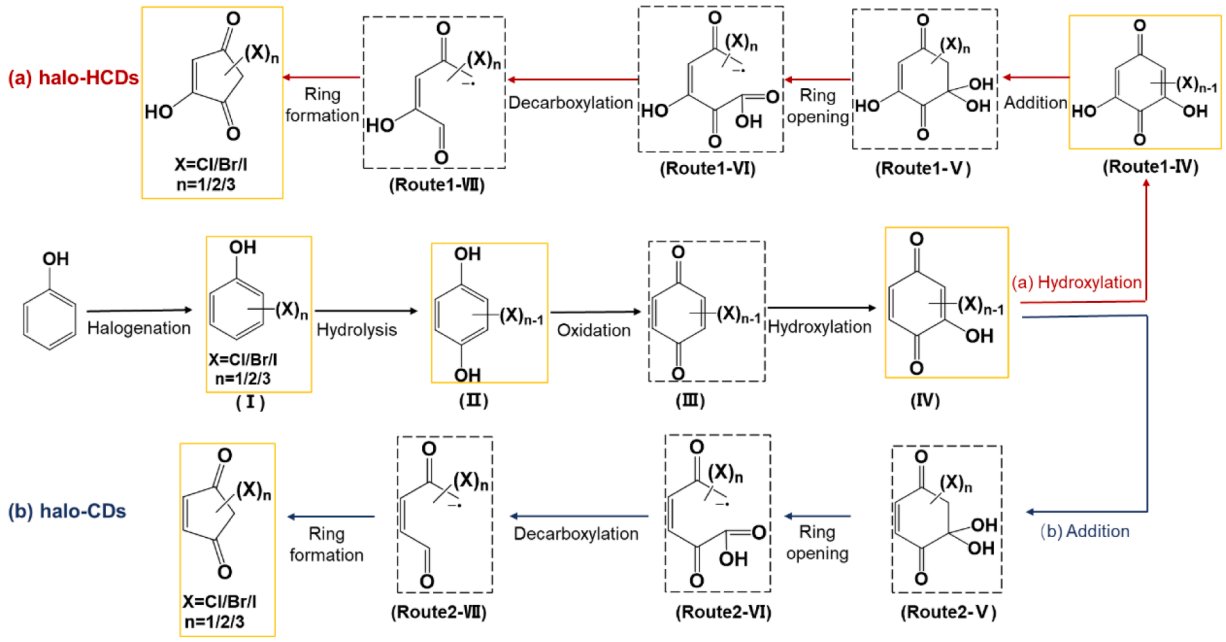

Fig. 5. Proposed formation pathways of (a) halo-HCDs and (b) halo-CDs formed in HOX-treated Phe (X = Cl/Br/I, n = 1/2/3). Noted that the compounds in solid box have been identified while the ones in the dashed box are theoretically proposed.

generate halo-CDs. Detailed formation routes for representative halo-CDs (B2 and B5) were provided in Fig. S10(a, b). While the formation potentials of halo-CDs may vary among different phenolic types, their underlying formation mechanisms remain consistent across substitution patterns. Future quantitative comparisons using authentic standards will provide further insights into these structural effects once available.

4. Conclusions

This study revealed that reactions of phenols with secondary disinfectants (HOBr and HOI) generated a more diverse and abundant suite of known and unknown DBPs compared to those formed with HOCl. Through an integrated EDA approach, highly toxic halo-CDs were identified for the first time as critical toxicants produced in these often-overlooked yet important secondary disinfection pathways. Although halo-CDs may also form during chlorination, their chlorinated analogues are of less toxicological concern than those formed during secondary disinfection, due to their lower toxic potency and formation potential under primary disinfection conditions. The environmental relevance of these compounds was confirmed by their detection in both simulated and real source waters treated with secondary disinfectants. Based on the identified halo-CD structures and key intermediates, a formation pathway was proposed, involving sequential steps of electrophilic halogenation, hydrolysis, and ring rearrangement. Computational toxicity assessment indicated that the identified halo-CDs possessed considerable predicted developmental toxicity, alongside potential risks for skin sensitization, carcinogenicity, and mutagenicity. These findings collectively highlighted that the formation of potent toxic by-products during secondary disinfection necessitates increased scrutiny in future water safety evaluations and regulatory frameworks.

CRediT authorship contribution statement

Mengge Fan: Writing – original draft, Visualization, Validation, Software, Methodology, Investigation, Data curation, Conceptualization. **Jialing Luo:** Software, Formal analysis. **Yanpeng Gao:** Software, Formal analysis. **Huang Huang:** Resources, Formal analysis. **Junlang Qiu:** Writing – review & editing, Supervision, Resources, Funding acquisition, Conceptualization. **Xin Yang:** Writing – review & editing, Supervision, Resources, Funding acquisition, Conceptualization.

Declaration of competing interest

The authors declare that they have no known competing financial interests or personal relationships that could have appeared to influence the work reported in this paper.

Acknowledgements

This work was supported by the National Natural Science Foundations of China (42307308, 22376226, 22561160125, 22425607).

Supplementary materials

Supplementary material associated with this article can be found, in the online version, at doi:10.1016/j.watres.2026.125875.

Data availability

Data will be made available on request.

References

Ayatollahi, S., Kalnina, D., Song, W., Cottrell, B.A., Gonsior, M., Cooper, W.J., 2012. Recent advances in structure and reactivity of dissolved organic matter: radiation chemistry of non-isolated natural organic matter and selected model compounds. Water. Sci. Technol. 66 (9), 1941–1949.

Bichsel, Y., Von Gunten, U., 2000. Hypoiodous acid: kinetics of the buffer-catalyzed disproportionation. Water. Res. 34 (12), 3197–3203.

Bond, T., Goslan, E.H., Parsons, S.A., Jefferson, B., 2012. A critical review of trihalomethane and haloacetic acid formation from natural organic matter surrogates. Environ. Technol. Rev. 1 (1), 93–113.

Boyce, S.D., Hornig, J.F., 1983. Reaction pathways of trihalomethane formation from the halogenation of dihydroxyaromatic model compounds for humic acid. Env. Sci. Technol. 17 (4), 202–211.

Brack, W., 2003. Effect-directed analysis: a promising tool for the identification of organic toxicants in complex mixtures? Anal. Bioanal. Chem. 377 (3), 397–407.

Chaidou, C.I., Georgakilas, V.I., Stalikas, C., Saraçi, M., Lahaniatis, E.S., 1999. Formation of chloroform by aqueous chlorination of organic compounds. Chemosphere 39 (4), 587–594.

Chang, E.E., Chiang, P.C., Chao, S.H., Lin, Y.L., 2006. Relationship between chlorine consumption and chlorination by-products formation for model compounds. Chemosphere 64 (7), 1196–1203.

Chuang, Y.H., Mccurry, D.L., Tung, H.H., Mitch, W.A., 2015. Formation pathways and trade-offs between haloacetamides and haloacetaldehydes during combined chlorination and chloramination of lignin phenols and natural waters. Env. Sci. Technol. 49 (24), 14432–14440.
Chowdhury, S., 2022. Effects of seawater intrusion on the formation of disinfection byproducts in drinking water. Sci. Total. Environ. 827, 154398.
Connolly, C.T., Cardenas, M.B., Burkart, G.A., Spencer, R.G.M., Mcclelland, J.W., 2020. Groundwater as a major source of dissolved organic matter to Arctic coastal waters. Nat. Commun. 11 (1), 1479.
Criquet, J., Rodriguez, E.M., Allard, S., Wellauer, S., Salhi, E., Joll, C.A., Von Gunten, U., 2015. Reaction of bromine and chlorine with phenolic compounds and natural organic matter extracts – Electrophilic aromatic substitution and oxidation. Water. Res. 85, 476–486.
Danish(Q)Sar, 2015. http://qsar.food.dtu.dk/.
Dejaeger, K., Criquet, J., Vanoppen, M., Vignal, C., Billon, G., Cornelissen, E.R., 2022. Identification of disinfection by-product precursors by natural organic matter fractionation: a review. Env. Chem Lett. 20 (6), 3861–3882.
Dong, H., Cuthbertson, A.A., Richardson, S.D., 2020. Effect-directed analysis (EDA): a promising tool for nontarget identification of unknown disinfection byproducts in drinking water. Env. Sci. Technol. 54 (3), 1290–1292.
Dong, H., Qiang, Z., Richardson, S.D., 2019. Formation of iodinated disinfection byproducts (I-DBPs) in drinking water: emerging concerns and current issues. Acc. Chem. Res. 52 (4), 896–905.
Dorji, P., Kim, D.I., Hong, S., Phuntsho, S., Shon, H.K., 2020. Pilot-scale membrane capacitive deionisation for effective bromide removal and high water recovery in seawater desalination. Desalination 479, 114309.
Fan, M., Yang, X., Kong, Q., Lei, Y., Zhang, X., Aghdam, E., Yin, R., Shang, C., 2022. Sequential ClO_2-UV/chlorine process for micropollutant removal and disinfection byproduct control. Sci. Total. Environ. 806, 150354.
Fang, C., Luan, X., Ao, F., Wang, X., Ding, S., Du, Z., Liu, S., Jia, R., Chu, W., 2023. Decomposition of total organic halogen formed during chlorination: the iceberg of halogenated disinfection byproducts was previously underestimated. Env. Sci. Technol. 57 (3), 1433–1442.
Gallard, H., Von Gunten, U., 2002. Chlorination of phenols: kinetics and formation of chloroform. Env. Sci. Technol. 36 (5), 884–890.
Gallard, H., Pellizzari, F., Croué, J.P., Legube, B., 2003. Rate constants of reactions of bromine with phenols in aqueous solution. Water. Res. 37 (12), 2883–2892.
Han, J., Zhang, X., Jiang, J., Li, W., 2021. How much of the total organic halogen and developmental toxicity of chlorinated drinking water might be attributed to aromatic halogenated DBPs? Env. Sci. Technol. 55 (9), 5906–5916.
Harkness, J.S., Dwyer, G.S., Warner, N.R., Parker, K.M., Mitch, W.A., Vengosh, A., 2015. Iodide, bromide, and ammonium in hydraulic fracturing and oil and gas wastewaters: environmental implications. Env. Sci. Technol. 49 (3), 1955–1963.
Heasley, V.L., Anderson, M.E., Combes, D.S., Elias, D.S., Gardner, J.T., Hernandez, M.L., Moreland, R.J., Shellhamer, D.F., 1993. Investigations of the structure and reactions of the intermediate in the chlorination of resorcinol. Environ. Toxicol. Chem. 12 (9), 1653–1659.
Heeb, M.B., Criquet, J., Zimmermann-Steffens, S.G., Von Gunten, U., 2014. Oxidative treatment of bromide-containing waters: formation of bromine and its reactions with inorganic and organic compounds — a critical review. Water. Res. 48, 15–42.
Hua, G., Reckhow, D.A., Kim, J., 2006. Effect of bromide and iodide ions on the formation and speciation of disinfection byproducts during chlorination. Env. Sci. Technol. 40 (9), 3050–3056.
Huang, Y., Li, H., Zhou, Q., Li, A., Shuang, C., Xian, Q., Xu, B., Pan, Y., 2018. New phenolic halogenated disinfection byproducts in simulated chlorinated drinking water: identification, decomposition, and control by ozone-activated carbon treatment. Water. Res. 146, 298–306.
Hung, Y.C., Waters, B.W., Yemmireddy, V.K., Huang, C.H., 2017. pH effect on the formation of THM and HAA disinfection byproducts and potential control strategies for food processing. J. Integr. Agric. 16 (12), 2914–2923.
Kimura, S.Y., Cuthbertson, A.A., Byer, J.D., Richardson, S.D., 2019. The DBP exposome: development of a new method to simultaneously quantify priority disinfection by-products and comprehensively identify unknowns. Water. Res. 148, 324–333.
Lee, Y., Yoon, J., Von Gunten, U., 2005. Kinetics of the oxidation of phenols and phenolic endocrine disruptors during water treatment with ferrate (Fe(VI)). Env. Sci. Technol. 39 (22), 8978–8984.
Li, J., Jiang, J., Pang, S.Y., Cao, Y., Zhou, Y., Guan, C., 2020. Oxidation of iodide and hypoiodous acid by non-chlorinated water treatment oxidants and formation of iodinated organic compounds: a review. Chem. Eng. J. 386, 123822.
Liu, C., Shin, Y.H., Wei, X., Ersan, M.S., Wagner, E., Plewa, M.J., Amy, G., Karanfil, T., 2022. Preferential halogenation of algal organic matter by iodine over chlorine and bromine: formation of disinfection byproducts and correlation with toxicity of disinfected waters. Env. Sci. Technol. 56 (2), 1244–1256.
Liu, J., Zhang, X., 2014. Comparative toxicity of new halophenolic DBPs in chlorinated saline wastewater effluents against a marine alga: halophenolic DBPs are generally more toxic than haloaliphatic ones. Water. Res. 65, 64–72.
Liu, S., Li, Z., Dong, H., Goodman, B.A., Qiang, Z., 2017. Formation of iodo-trihalomethanes, iodo-acetic acids, and iodo-acetamides during chloramination of iodide-containing waters: factors influencing formation and reaction pathways. J. Hazard. Mater. 321, 28–36.
Lu, Y., Wu, D.X., Ye, B., Du, Y., Wu, Q.Y., 2025. Comparative nontargeted analysis and toxicity of brominated disinfection byproducts from chlorination and chloramination of natural organic matter. Env. Sci. Technol. 59 (25), 12990–12999.
Mccomas, C.C., Perales, J.B., Van Vranken, D.L., 2002. Synthesis of (±)-madindolines and chemical models. Studies of chemical reactivity. Org. Lett. 4 (14), 2337–2340.
Ouyang, J., Lin, M., Wei, F., Ling, C., Lu, T., Liu, Y., Qi, B., Hu, J., He, J., Zhuang, G., 2024. Estimation of suspected estrogenic transformation products generated during preservative butylparaben chlorination using a simplified effect-based analysis approach. Water. Res. 267, 122414.
Pan, X., Li, D., Song, H., Chen, Q., Yan, Q., Zhou, C., Huang, X., Xin, Y., Liu, G., Ma, J., 2021. Investigating the formation of iodinated aromatic disinfection by-products in chlorine/phenol/iodide system. Sci. Total. Environ. 797, 149152.
Pan, Y., Li, W., Li, A., Zhou, Q., Shi, P., Wang, Y., 2016. A new group of disinfection byproducts in drinking water: trihalo-hydroxy-cyclopentene-diones. Env. Sci. Technol. 50 (14), 7344–7352.
Postigo, C., Zonja, B., 2019. Iodinated disinfection byproducts: formation and concerns. Curr. Opin. Environ. Sci. Health 7, 19–25.
Qiao, Y., Feng, J., Liu, X., Wang, W., Zhang, P., Zhu, L., 2016. Surface water pH variations and trends in China from 2004 to 2014. Env. Monit. Assess. 188 (7), 443.
Ritchie, J.D., Perdue, E.M., 2003. Proton-binding study of standard and reference fulvic acids, humic acids, and natural organic matter. Geochim. Cosmochim. Acta 67 (1), 85–96.
Rosenberg, S.A., Nikolov, N.G., Dybdahl, M., Simmons, S., Crofton, K.M., Watt, E.D., Friedmann, K.P., Judson, R.S., Wedebye, E.B., 2016. Development of a QSAR Model for thyroperoxidase inhibition and screening of 72,526 REACH substances. In: Abstract from Sustain-ATV Conference 2016. Kgs. Lyngby, Denmark.
Sharma, N., Karanfil, T., Westerhoff, P., 2019. Historical and future needs for geospatial iodide occurrence in surface and groundwaters of the United States of America. Env. Sci. Techn. Lett. 6 (7), 379–388.
Tee, O.S., Paventi, M., Bennett, J.M., 1989. Kinetics and mechanism of the bromination of phenols and phenoxide ions in aqueous solution. Diffusion-controlled rates. J. Am. Chem. Soc. 111 (6), 2233–2240.
Wagner, E.D., Plewa, M.J., 2017. CHO cell cytotoxicity and genotoxicity analyses of disinfection by-products: an updated review. J. Env. Sci. 58, 64–76.
Wang, Y., Le Roux, J., Zhang, T., Croué, J.P., 2014. Formation of brominated disinfection byproducts from natural organic matter isolates and model compounds in a sulfate radical-based oxidation process. Env. Sci. Technol. 48 (24), 14534–14542.
Westerhoff, P., Chao, P., Mash, H., 2004. Reactivity of natural organic matter with aqueous chlorine and bromine. Water. Res. 38 (6), 1502–1513.
Yang, M., Zhang, X., 2013. Comparative developmental toxicity of new aromatic halogenated DBPs in a chlorinated saline sewage effluent to the marine polychaete platynereis dumerilii. Env. Sci. Technol. 47 (19), 10868–10876.
Yang, W., Bond, T., Fang, C., Du, Z., Chu, W., 2025. High molecular-weight organics as precursors for toxic iodinated disinfection byproducts during chloramination. Env. Sci. Technol. 59 (2), 1378–1387.
Yang, Y., Komaki, Y., Kimura, S.Y., Hu, H.Y., Wagner, E.D., Mariñas, B.J., Plewa, M.J., 2014. Toxic impact of bromide and iodide on drinking water disinfected with chlorine or chloramines. Env. Sci. Technol. 48 (20), 12362–12369.
Zhao, Y., Anichina, J., Lu, X., Bull, R.J., Krasner, S.W., Hrudey, S.E., Li, X.F., 2012. Occurrence and formation of chloro-and bromo-benzoquinones during drinking water disinfection. Water. Res. 46 (14), 4351–4360.
Zhong, Y., Gan, W., Du, Y., Huang, H., Wu, Q., Xiang, Y., Shang, C., Yang, X., 2019. Disinfection byproducts and their toxicity in wastewater effluents treated by the mixing oxidant of ClO_2/Cl_2. Water. Res. 162, 471–481.
Zhu, X., Zhang, X., 2016. Modeling the formation of TOCl, TOBr and TOI during chlor (am) ination of drinking water. Water. Res. 96, 166–176.